ACS OMEGA

Article

Cite This: ACS Omega 2018, 3, 13211−13218

http://pubs.acs.org/journal/acsodf

Subgram-Scale Synthesis of Biomass Waste-Derived Fluorescent Carbon Dots in Subcritical Water for Bioimaging, Sensing, and Solid-State Patterning

Rina Su,[†,‡] Dan Wang,[*,†] Mei Liu,[§] Jia Yan,[§] Jie-Xin Wang,[†,‡] Qiuqiang Zhan,[∥] Yuan Pu,[*,‡] Neil R. Foster,[†,⊥] and Jian-Feng Chen[†,‡]

[†]State Key Laboratory of Organic-Inorganic Composites and [‡]Research Centre of the Ministry of Education for High Gravity Engineering and Technology, Beijing University of Chemical Technology, Beijing 100029, China

[§]Jiangsu Key Laboratory of Oral Diseases, Nanjing Medical University, Nanjing, Jiangsu 210029, China

[∥]Centre for Optical and Electromagnetic Research, South China Academy of Advanced Optoelectronics, South China Normal University, Guangzhou 510006, China

[⊥]Department of Chemical Engineering, Curtin University, Perth, Western Australia 6845, Australia

Supporting Information

ABSTRACT: Fluorescent carbon dots (FCDs) have received considerable attention because of the great potential for a wide range of applications, from bioimaging to optoelectronic devices. In this work, we reported the synthesis of nitrogen-doped FCDs with an average size of 2 nm in a subcritical water apparatus by using biomass waste (i.e., expired milk) as the precursor. The obtained FCDs were highly dispersed in aqueous solution because of the presence of O-containing functional groups on their surfaces. Under the excitation of ultraviolet and blue light, the FCDs exhibited excitation wavelength-dependent fluorescence in the emission range of 400−550 nm. The FCDs could be easily taken up by HeLa cells without additional surface functionalization, serving as fluorescent nanoprobes for bioimaging. The applications of FCDs as sensing agents for the detection of Fe^{3+}, solid-state fluorescent patterning, and transparent hybrid films were also performed, demonstrating their potential for solid-state fluorescent sensing, security labeling, and wearable optoelectronics.

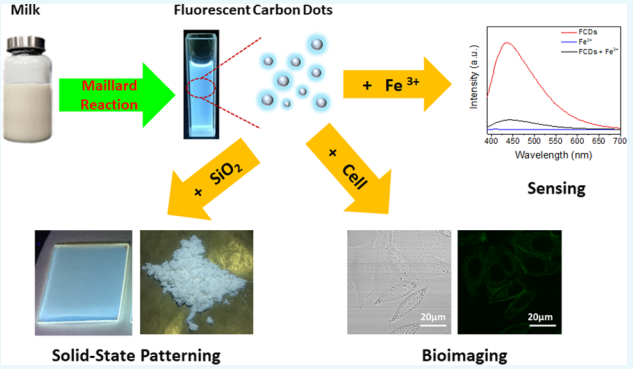

INTRODUCTION

Fluorescent nanomaterials have received intense scientific attention and offer promising applications from molecular sensors through cancer diagnosis agents to optoelectronic devices.[1−4] Fluorescent carbon dots (FCDs), also known as carbon quantum dots or carbon nanodots, are among the most attractive of fluorescent nanomaterials, offering low cytotoxicity, favorable biocompatibility, and high photostability.[5−8] Consequently, a variety of synthetic strategies for FCDs have been developed, which can be classified into top-down and bottom-up approaches.[9−11] The top-down approach involves the cleavage of carbonaceous materials via acidic oxidation, hydrothermal treatment, or electrochemical exfoliation of carbon materials, such as graphite, graphene, carbon nanotubes, and carbon black.[12−14] However, the top-down approach requires expensive machines and high energy consumption, which limited the scale-up production of FCDs.[15] Alternatively, the bottom-up approach for the synthesis of FCDs is based on solution chemistry, cyclodehydrogenation of polyphenylene precursors, or carbonization of certain polymers.[16] In particular, the use of biomass as precursors for the preparation of FCDs has attracted much attention as an effective method for the mass production of FCDs because of the low cost and ease of scale-up.[17−21]

Milk as one of the most popular sources of nutrition for human beings is an emulsion or colloid of butterfat globules containing carbohydrates and proteins in general.[22] Millions of tons of milk are produced everyday throughout the world, and people are always willing to drink fresh milk than that past the sell-by date in most countries. Therefore, retailers and consumers discard billions of dollars of unspoiled milk each year while relying on inaccurate printed expiration dates. Along with others, we have found that milk can be used as a mutual precursor of carbon and nitrogen for the synthesis of nitrogen-doped FCDs,[23−25] which offers an effective way to turn waste into wealth. However, the previous reported microwave-

Received: August 6, 2018
Accepted: October 1, 2018
Published: October 15, 2018

DOI: 10.1021/acsomega.8b01919
ACS Omega 2018, 3, 13211−13218

assisted approaches or hydrothermal methods suffer from multiple disadvantages for scale-up,[26] including high energy consumption of the microwave process and high cost of the Teflon-lined autoclaves that are used as reactors. The high-pressure reactors widely used in the supercritical/subcritical fluid technique can generate subcritical water (SBCW) referring to liquid water, with pressure in the temperature range of 373.15−647.15 K,[27] which provides a good reaction condition for FCD synthesis from milk in theory. The uses of the SBCW apparatus in various fields such as chemical reaction, extraction, and material processing have been realized in laboratory scale and even in large-scale industrial applications.[28−30] However, as far as we are aware, few studies have been focused on the synthesis of FCDs in SBCW apparatuses.

In this work, we reported the preparation of FCDs using milk (3 days overdue) as the carbon precursor in SBCW. The obtained FCDs showed an average size of 2 nm, with a large amount of functional groups such as −COOH and −OH, and N-containing groups, which made them well-dispersed in aqueous solution. The optical characterization showed that the FCDs exhibited an excitation wavelength-dependent emission in the wavelength range of 400−550 nm. Compared with the commonly used hydrothermal or microwave-assisted synthesis methods, the methodology developed in the present study has the following advantages: (1) it offers a means to use one facility's waste (expired milk) as another's input, thereby reducing the raw materials required and waste generated; (2) the reaction process developed in the SBCW apparatus is more convenient for real-time monitoring of the temperature and pressure in the reaction system and more reliable for scalable mass production; (3) the newly developed FCDs show important potential in many application areas such as solid-state fluorescent sensing, security labeling, and wearable optoelectronics. We also demonstrated the applications of the obtained FCDs in the fluorescence sensing of Fe^{3+} and as fluorescent inks for patterning. Further, this paper also presented an easy and effective method for synthesizing FCDs/SiO_2 nanocomposites to prevent the self-quenching of FCDs in solid state.

RESULTS AND DISCUSSION

Synthesis and Characterization of FCDs. The expired milk was pumped into the microreactor (MR) of the SBCW apparatus, as shown in Figure 1. The nitrogenous proteins in the milk were then transformed into FCDs during the hydrothermal treatment in SBCW. The use of biomass waste (i.e., expired milk) as the nitrogen and carbon precursor offered a means to use one facility's waste as another's input, thereby reducing the raw materials required and waste generated. Compared with the conventional Teflon-lined autoclaves used for the hydrothermal synthesis of FCDs, the SBCW apparatuses with a temperature probe and pressure controller are more convenient for real-time monitoring and controlling of the temperature and pressure in the reaction system. In addition, by coupling with a freeze-drying equipment, the yield of FCDs could be largely improved. Therefore, the newly developed synthesis method is more suitable for mass production and industrial applications.

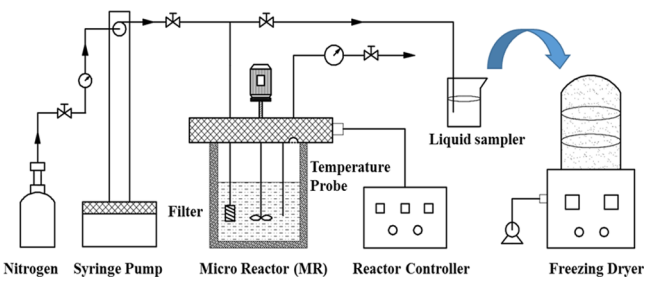

Figure 1. Schematic diagram of the SBCW apparatus coupled with a freeze dryer.

Figure 2 illustrates the possible process for the formation of FCDs from milk in SBCW. The proteins in the solution were folded within three-dimensional domains in the precursor. When the temperature of the solution grew up, protein denaturation occurred.[31] The amino acids were unraveled, followed by the hydrolysis of proteins over 60 °C in the SBCW apparatus.[32] The reactions between the amine group compounds and carboxides in the solution then occurred, similar to the Maillard reaction, forming polymer-like dots.[33] The formation of nanosized spherical FCDs was attributed to the self-assembly of the polymer-like dots. The powder of FCDs can be easily obtained by freeze-drying treatment.

Figure 3a shows the subgram-scale (768.4 mg) quantities of dried FCD powders in one batch in our experiments (Figure S1). The FCDs could be easily dispersed in aqueous solution (Figure S2). Figure 3b shows a typical transmission electron microscopy (TEM) image of the obtained FCDs. The FCDs exhibited a spherical shape and were highly monodispersed with no significant aggregates observed. The diameters of the FCDs were less than 5 nm, with uniform size distributions. The corresponding nanoparticle size distribution histogram was obtained by counting about 150 FCDs (the inset of Figure 3b). The crystallinity of the FCDs was evaluated by X-ray diffraction (XRD) measurements (Figure S3), from which a broad peak of ultrasmall carbon dots was observed. To study the components and structures of the FCDs, both the Fourier transform infrared spectroscopy (FTIR) and X-ray photoelectron spectroscopy (XPS) spectra were then examined. The FTIR spectrum in Figure 3c reveals the characteristic absorption bands of the O−H and N−H stretching vibrations in the region of 3020−3700 cm^{-1}, along with the characteristic band of C−H stretching vibration at 2940 cm^{-1}. The C═O and C═C stretching vibrations were recorded at 1680 and 1597 cm^{-1}, whereas the C−N stretching vibration was found at 1400 cm^{-1}. The broad band around 1070 cm^{-1} was attributed to the C−O bending vibration.[34] The XPS full survey spectrum presented in Figure 3d shows three typical peaks: C 1s (285 eV), N 1s (400 eV), and O 1s (532 eV), which indicate that the FCDs composed of carbon, nitrogen, and oxygen. In the high-resolution spectra (Figure 3e,f), the C 1s band can be deconvoluted into four peaks at 284.7, 286.1, 287.6, and 288.7 eV, corresponding to the C 1s states in C−C/C═C, C−N/C−O, C═O, and COOH, respectively. The N 1s spectrum exhibits two peaks at 399.6 and 401.2 eV, representing pyrrolic N and graphite N. The O 1s band in Figure S4 contains two peaks at 531.3 and 532.4 eV for C═O and C−O, respectively.[35] These results demonstrated the presence of abundant functional groups like −COOH and −OH, and N-containing groups, in the milk-derived FCDs, enabling them to be well-dispersed in aqueous solution for various applications.

The UV−visible absorption spectrum of the aqueous dispersion of FCDs (Figure 4a) shows a sharp absorbance peak at 280 nm, which is attributed to the aromatic π orbital

DOI: 10.1021/acsomega.8b01919
ACS Omega 2018, 3, 13211−13218

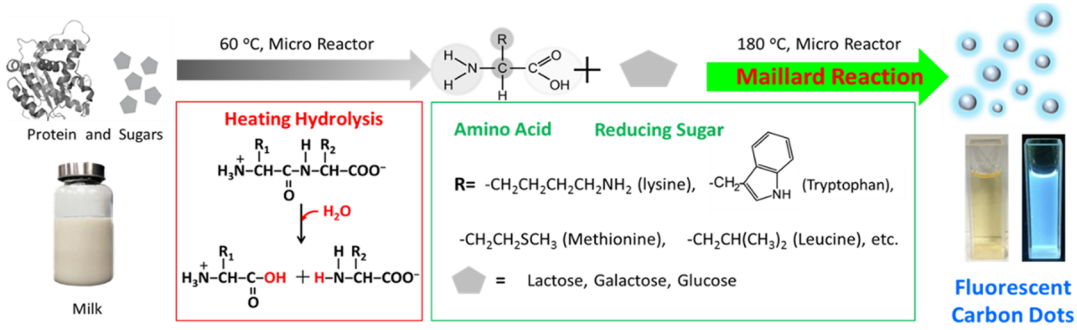

Figure 2. Schematic diagram for the route to FCDs from milk by the hydrolysis of protein and subsequent Maillard reaction in SBCW.

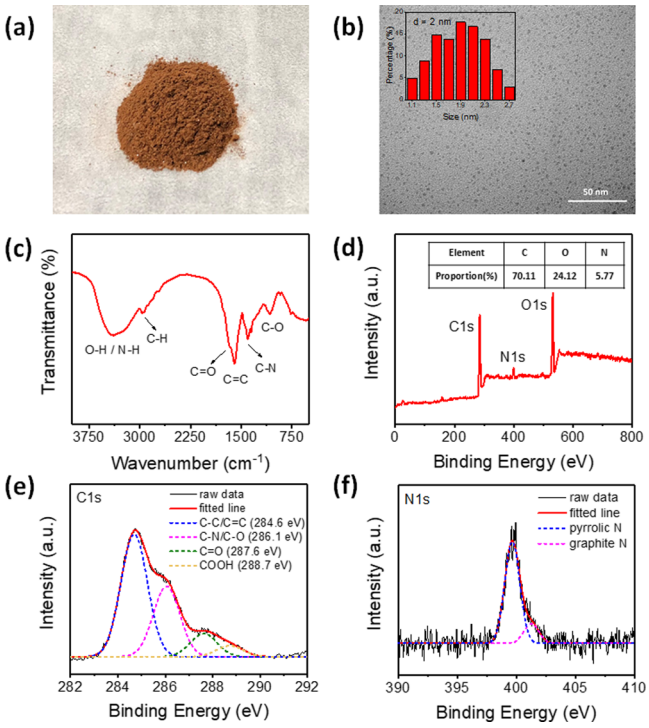

Figure 3. (a) Typical picture of dried FCD powder in one batch reaction. (b) Typical TEM image of FCDs (inset: size distribution histogram). (c) FTIR spectrum of the FCDs. (d) XPS spectrum of the FCDs. (e–f) High-resolution XPS C 1s and N 1s spectra of the FCDs.

electron transition of the nanocarbon structure.[36] Figure 4a also shows the FCDs obtained by expired milk exhibiting a high fluorescence emission band at 440 nm when it was excited by 360 nm, the fluorescence intensity of which is comparable with that of normal milk (Figure S5). Upon irradiation with a 365 nm UV light, the FCDs can generate a blue color (Figure 4a inset). These prepared FCDs have an excitation-dependent emission property, as shown in Figure 4b, that the emission peaks shift to a longer wavelength with the increase of the excitation wavelength, and this phenomenon may be caused by the optical selection of different defect states on the surface of CDs.[37] We also noticed that the fluorescence quantum yield (QY) of carbon dots is 8.64%, and this value is higher than that of some of the previously reported carbon dots which use biomass as the precursor.[38−41] In addition, to explore the effect of temperature on the fluorescence behavior, the FCDs were examined at different temperatures (0, 30, and 60 °C). Figure 4c shows the result that the lower the temperature, the stronger is the fluorescence intensity in a certain temperature range.

In Vitro Cytotoxicity. To ensure the potential of the FCDs for biorelated applications, the cytotoxicity of the FCDs was investigated toward HeLa cells and mouse bone marrow mesenchymal stem cells (BMSCs) P2 by a typical CCK-8 assay. Figure 5a shows the relative cell viability of HeLa cells treated with different concentrations of the FCDs. We can see that no significant cytotoxicity of cells was caused by the FCDs, even at high concentrations of 300 μg/mL. Further, Figure 5b shows the relative cell viability for the mouse BMSCs P2 treated with the synthesized FCDs at different concentrations for 0, 12, 24, and 48 h. We can see that after 48 h, the cells still have high cell viability, even at high concentrations of 400 μg/mL, which confirms that the FCDs are cytocompatible and do not induce cell death.

In Vitro Cell Imaging. Taking advantage of the scalable synthesis approach and the desired optical property, we then demonstrated the as-prepared FCDs to be a promising

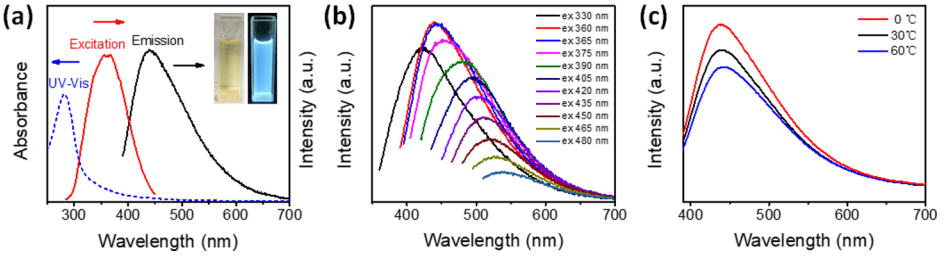

Figure 4. (a) UV−visible absorption (blue line), fluorescence excitation (red line), and emission (black line) spectra of the FCDs (λ_{ex} = 360 nm, λ_{em} = 440 nm). The inset shows the photographs of the FCDs in aqueous solutions under daylight irradiation (left) and a 365 nm UV lamp excitation (right). (b) Emission spectra of the FCDs at different excitation wavelengths from 330 to 480 nm. (c) Fluorescent spectra of the FCDs at different temperatures (λ_{ex} = 360 nm).

DOI: 10.1021/acsomega.8b01919
ACS Omega 2018, 3, 13211−13218

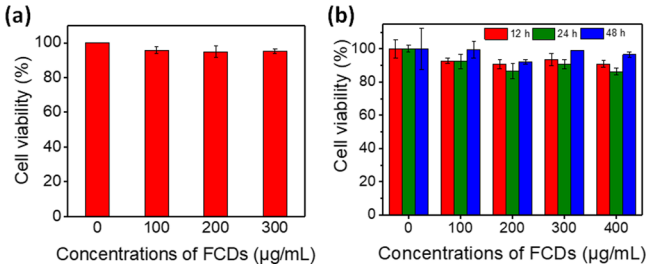

Figure 5. Cell viability by CCK-8 assay of (a) HeLa cells incubated with different concentrations of the FCDs for 6 h and (b) mouse BMSCs P2 treated with the synthesized FCDs at different concentrations for 0, 12, 24, and 48 h.

nanoprobe for fluorescent cellular imaging. Figure 6a,b shows the images of control cells (without FCD treatment) and

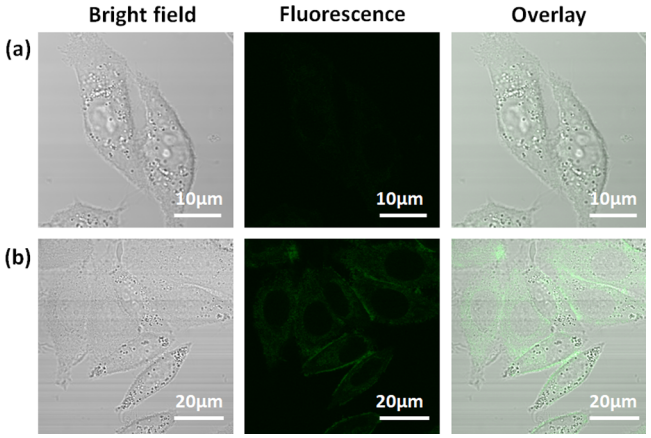

Figure 6. Two-photon excited fluorescence imaging of HeLa cells. (a) Control cells without FCD treatment and (b) cells incubated with 200 μg/mL of FCDs for 6 h.

experimental cells (incubated with 200 μg/mL of FCDs for 6 h). According to the bright-field images, the morphologies of both control cells and experimental cells were kept very well, indicating the FCDs did not cause significant toxicity to the cells. The fluorescence images illustrated that the two-photon excited fluorescence of FCDs could be clearly observed from the cytoplasm of the cells. As the cells were irradiated by a 780 nm femtosecond laser for fluorescence imaging, no auto-fluorescence of the cells was detected. These results demonstrated the efficient uptake of FCDs by HeLa cells, making them promising candidates as cellular imaging agents and drug carriers in biomedical research.

Fluorescent Sensing of Fe^{3+}. Interestingly, we can see the fluorescence quench obviously upon the addition of 2 mM Fe^{3+} in Figure 7a, and the inner filter effect of Fe^{3+} for the fluorescent quenching of FCDs was excluded (Figure S6). The quenching efficiency was calculated to be about 76.57%. From recent reports, the existence of abundant oxygen-containing functional groups on the surface of FCDs might be the reason for the FCDs to be able to detect Fe^{3+}.[42,43] The UV−visible absorption spectrum in Figure 7b shows that FCDs exhibit an obvious absorption band at 280 nm and that the Fe^{3+} aqueous solution displays a strong absorption at 290 nm. When 2 mM Fe^{3+} was added into the FCDs, the absorption peak of FCDs increased evidently, and Fe^{3+} disappeared. Further, comparing the experiment-determined UV absorption of the FCD/Fe^{3+}

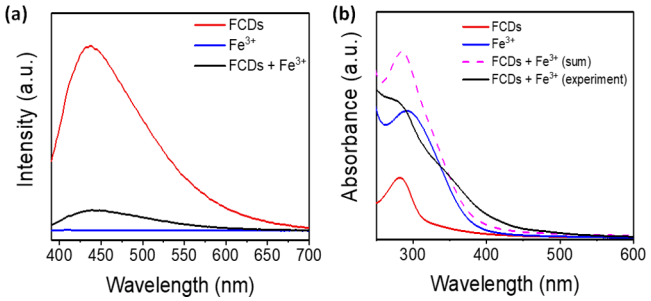

Figure 7. (a) Fluorescence emission spectra of the FCDs, Fe^{3+}, and FCDs + Fe^{3+} (λ_{ex} = 360 nm). (b) UV−visible absorption spectra of the FCDs, Fe^{3+}, and FCDs + Fe^{3+}.

solution (black line in Figure 7b) with the sum of individual absorptions from FCDs and Fe^{3+} (pink line in Figure 7b) at the same concentrations, it was observed that they were not similar, which indicated that the reaction happened between the FCDs and Fe^{3+} to form the FCDs/Fe^{3+} complex.

As shown in Figure 8a,b, the results display the excellent sensitivity of the detection of Fe^{3+}. The fluorescence intensity of FCDs obviously quenched with the increase of the concentration of Fe^{3+} from 0.0 to 2.0 mM. In addition, a good linear correlation is found between the fluorescence quenching efficiency (F_0/F) of FCDs and the Fe^{3+} concentration in the range of 0.5−1.4 mM. The concentration of Fe^{3+} can be calculated by the following equation

$$\frac{F_0}{F} = 3.520C\ (\mathrm{mM}) + 0.294\ (R^2 = 0.996) \quad (1)$$

where F_0 and F correspond to the fluorescence intensities of FCDs before or after adding Fe^{3+}, respectively, and C represents the concentration of Fe^{3+}.

To determine whether the proposed strategy is selective for Fe^{3+} sensing, 13 other common cations were also investigated. Operationally, these 13 common cations including Ba^{2+}, Cd^{2+}, Mn^{2+}, Na^{+}, Mg^{2+}, K^{+}, Ca^{2+}, NH_4^{+}, Al^{3+}, Zn^{2+}, Pb^{2+}, Ni^{2+}, and Co^{2+} were tested for the same conditions in the presence of 2 mM Fe^{3+}. By comparing ($F_0 - F$) of Fe^{3+} with those of the other targets in Figure 8c (F_0 and F correspond to the fluorescence intensity of FCDs before or after adding these common cations), it is not hard to find that only Fe^{3+} induce obvious quenching, whereas other cations display little quenching effect, which forcefully suggests that the as-prepared FCDs in SBCW have high selectivity toward Fe^{3+} over the other relevant cations. These results prove that the FCDs prepared in SBCW have high sensitivity and outstanding selectivity for Fe^{3+} sensing.

Fluorescent Ink for Patterning. Because of the bright fluorescence of FCDs, they were also used as inks for drawing patterns. The FCDs were dissolved in water because of their excellent water solubility aforementioned. After drawing (Figure 9a), the FCDs patterns closely attached on the paper and gave significant fluorescence spectrum under a 365 nm UV lamp excitation (Figure 9b), whereas the paper showed a negligible background UV fluorescence (Figure 9c), and the fluorescence peak of the FCDs in the solid state is the same as that of the FCDs in solution, at 440 nm (Figure 4a). Many baseplates such as textiles, certain flexible plastic films, and even the skin of animals can be printed by FCDs because of the natural raw material milk and the nontoxic preparation process. Further, the FCD ink shows good photostability,

DOI: 10.1021/acsomega.8b01919
ACS Omega 2018, 3, 13211−13218

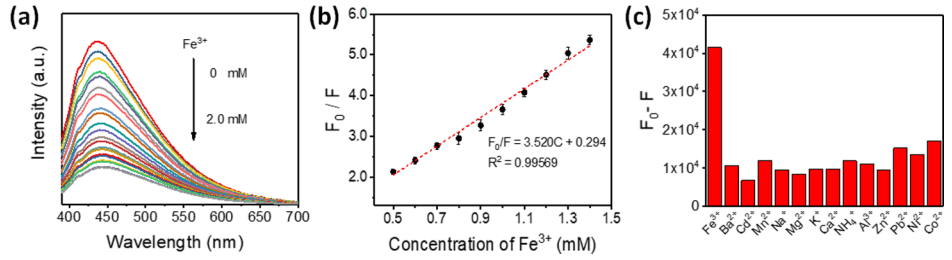

Figure 8. (a) Fluorescence emission spectra of the FCDs with different concentrations of Fe^{3+} (λ_{ex} = 360 nm). (b) Linear correlation of (F_0/F) vs the Fe^{3+} concentration in the range of 0.5−1.4 mM. (c) Fluorescence responses of the FCDs for the addition of different common cations, and the concentration of each cation is 2 mM (λ_{ex} = 360 nm).

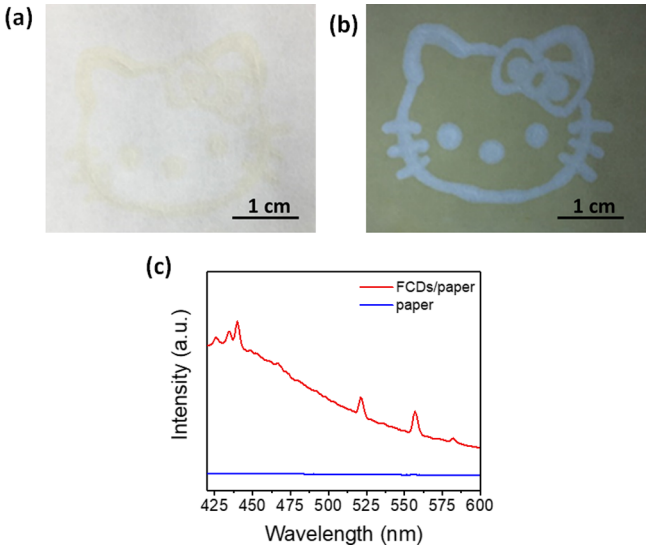

Figure 9. (a) Photographs of the FCD patterns drawn from the FCD ink under daylight and (b) 365 nm UV lamp excitation. (c) Fluorescence emission spectra of the FCDs in solid state and background fluorescence of the paper (λ_{ex} = 360 nm).

which can be seen from the pattern and fluorescence emission spectra after continuous irradiation under the UV lamp (365 nm) for 1 h (Figure S7), suggesting that the FCDs are promising for antifake labeling.

Preparation of FCDs/SiO_2 Nanocomposites. As a result of fluorescence quenching in solid state, there are no obvious fluorescence from FCD powders when illuminated by UV light (Figure S8). As shown in Figure 10a,b, blue emissions are visualized from the FCDs/SiO_2 nanocomposite films with different volumes of FCDs (200, 100, 50, and 0 μL) under a 365 nm UV lamp irradiation. The fluorescence spectra (Figure 10c) of FCDs/SiO_2 nanocomposite films with different volumes of FCDs were measured to further indicate that this method can restrain fluorescence quenching because the silica matrix was formed faster and the FCDs were embedded into silica by physical doping between the FCDs and silica.[44] Figures 10d,e, S9, and S10 show that the FCDs/SiO_2 nanocomposite powders also have blue fluorescence under a 365 nm UV lamp excitation. The FCDs/SiO_2 nanocomposites might be used in light-emitting diodes, which are potentially used in indoor lighting.

CONCLUSIONS

In conclusion, we have demonstrated the synthesis of nitrogen-doped FCDs in SBCW by using expired milk as the nitrogen and carbon precursor, offering a means to use one facility's

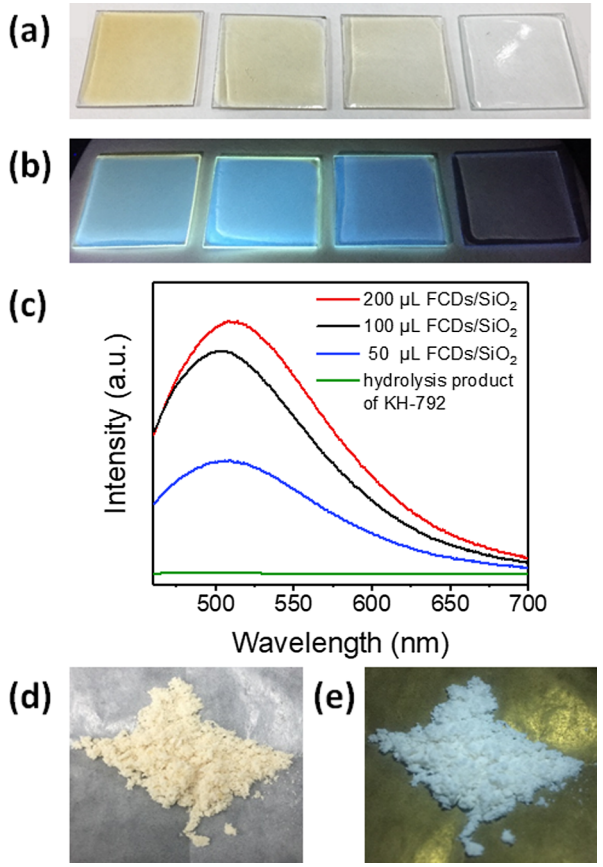

Figure 10. (a) Photographs of FCDs/SiO_2 nanocomposite films with different volumes of FCDs (11 mg/mL) under daylight and (b) 365 nm UV lamp excitation. (c) Fluorescence emission spectra of FCDs/SiO_2 nanocomposite films with different volumes of FCDs (11 mg/mL, λ_{ex} = 410 nm). (d) Photographs of FCDs/SiO_2 nanocomposite powders under daylight and (e) 365 nm UV lamp excitation.

waste (expired milk) as another's input, thereby reducing the raw materials required and waste generated. The reaction process in the SBCW apparatus was allowed for real-time monitoring of temperature and pressure, making the newly developed approaches suitable for scalable mass production. The prepared FCDs, with an average size of 2 nm, contained a large amount of functional groups like −COOH and −OH, and a handful of N-containing groups, displaying excellent water solubility and exhibiting strong excitation wavelength-dependent blue emission. Meanwhile, the FCDs have also been used for bioimaging, fluorescent sensing of Fe^{3+}, solid-state patterning, and transparent fluorescent hybrid composites,

DOI: 10.1021/acsomega.8b01919
ACS Omega 2018, 3, 13211−13218

showing the potential for solid-state fluorescent sensing, antifake labeling, and wearable optoelectronics.

EXPERIMENTAL SECTION

Materials. The milk products were purchased from the local supermarket and used as the precursor for the synthesis of FCDs when they were 3 days overdue. The other chemicals were purchased from Beijing Sinopharm Chemical Reagent Co., Ltd. and used as received. Deionized (DI) water was prepared by a Hitech Laboratory Water Purification System DW100 (Shanghai Hitech Instruments Co., Ltd.) and used for all experiments.

Synthesis of FCDs. The setup of the SBCW apparatus is similar to that of our previous reports.[45] Briefly, the MR was loaded with 20 mL of water and 25 mL of milk and then heated to a temperature of 180 °C using a heater, and the mixture was constantly stirred at 800 rpm for 2 h, which was controlled by the reactor controller. The system was maintained at a constant pressure of 1.2 MPa, which, ensuring water inside the apparatus, was in a subcritical state. Then, the FCDs were obtained by centrifuging (10 000 rpm for 20 min) and filtering through 0.22 μm Millipore syringe filters. The final product of the FCD powder was prepared by freeze-drying. It should be noted that no specific separation/purification processes were involved in our experiments, and the obtained FCDs have shown good performance in the applications including bioimaging, fluorescent sensing of Fe^{3+}, solid-state patterning, and transparent fluorescent hybrid composites (see the Results and Discussion section). Further purification may be needed for further potential applications such as super-resolution bioimaging and optoelectronic devices.

Characterization. The morphologies of the samples were observed by a Hitachi HT-7700 transmission electron microscope. The ultraviolet−visible (UV−vis) absorption spectra were characterized by a Shimadzu UV-2600 spectrophotometer. An Edinburgh Instruments FS5 fluorescence spectrometer was used to measure the fluorescence spectra of the samples. The FTIR spectra were recorded using a Thermo Fisher spectrum Nicolet 6700 FTIR instrument. A Thermo Fisher Scientific ESCALAB 250 XPS system was used for the analysis of the surface properties of the samples. The XRD patterns were obtained with a Rigaku 2500VB2+PC X-ray diffractometer. The fluorescence QY was acquired using an integrating sphere incorporated into an Edinburgh Instruments FLS980 spectrofluorometer.

Cell Viability Experiments. The cell viability experiments were performed using a Cell Counting Kit (CCK-8), which was purchased from Dojindo Laboratory, Japan. A total of 96 wells of HeLa cells were prepared, containing about 6×10^3 cells in each well. The HeLa cells were randomly separated into four groups. Three groups were treated with the synthesized FCDs at a concentration of 100, 200, and 300 μg/mL. The other group of HeLa cells included blank control cell lines without any treatment. After incubation for 6 h, 10 μL of CCK-8 was added to each well, and the HeLa cells were incubated for another 1 h. At the same time, the cell viability tests were further investigated by using mouse BMSCs P2. A total of 96 wells of mouse BMSCs P2 were prepared, containing about 2.5×10^3 cells in each well. Further, the mouse BMSCs P2 were separated into five groups. Four groups were treated with the synthesized FCDs at a concentration of 100, 200, 300, and 400 μg/mL. The other group of cells included the blank control cell lines without any treatment. All the groups were incubated for 0, 12, 24, and 48 h, respectively. The CCK-8 was mixed with the medium in a ratio of 1:10, and the mouse BMSCs P2 were incubated for another 2 h. The absorbance was measured at 450 nm. The cell viability of all the control cells was assumed to be 100%, and the relative viability of the cells treated with various samples was estimated. The whole experiment was repeated four times.

In Vitro Cell Imaging. HeLa cells were cultured in a Dulbecco's minimum essential media with 10% fetal bovine serum, 100 U/mL penicillin, and 100 μg/mL streptomycin. For fluorescence imaging, the untreated cells and those treated with FCDs (200 μg/mL) were examined. The cells were then incubated at 37 °C with 5% CO_2 for 6 h. Thereafter, all the cell samples were gently washed three times with phosphate-buffered saline and directly imaged using two-photon-excited fluorescence microscopy, using a 780 nm (40 mW) femtosecond laser irradiation.

Fluorescent Sensing of Fe^{3+}. The related experiments were conducted in a NaAc−HAc (10 mM) buffer solution to avoid the hydrolysis of Fe^{3+}. Typically, 300 μL of FCDs was added into 60 mL of NaAc−HAc, and then 2.5 mL of the FCDs of the (NaAc−HAc) solution and the same volume of Fe^{3+} (2 mM) were mixed and reacted for 5 min. For sensitivity study, different concentrations of Fe^{3+} within 2 mM were examined in the same way. The selectivity of Fe^{3+} detection was confirmed by adding a variety of positive ions including Ba^{2+}, Cd^{2+}, Mn^{2+}, Na^{+}, Mg^{2+}, K^{+}, Ca^{2+}, NH_4^{+}, Al^{3+}, Zn^{2+}, Pb^{2+}, Ni^{2+}, and Co^{2+} ions instead of Fe^{3+} (2 mM). The fluorescence emission spectrum was recorded at an excitation of 360 nm. The whole experiment was repeated three times.

Preparation of FCDs/SiO_2 Nanocomposites. FCDs (11 mg) were dissolved in 10 mL of DI water, and then different concentrations of FCDs (200, 100, 50, and 0 μL) were added into 500 μL of KH-792 and 2 mL of water. The mixtures were sonicated for 5 min to form homogeneous solutions. The FCDs/SiO_2 films and powders were obtained through a facile heating (80 °C) and grinding process.

ASSOCIATED CONTENT

Supporting Information

The Supporting Information is available free of charge on the ACS Publications website at DOI: 10.1021/acsomega.8b01919.

Product of the preparation of FCDs in one batch reaction; photograph of the water solubility test of the FCDs; XRD patterns of the FCDs; high-resolution XPS O 1s spectra of the FCDs; fluorescent spectra of the FCDs obtained by normal milk and expired milk; UV−visible absorption spectra with different concentrations of Fe^{3+}; fluorescence photograph and fluorescence emission spectra of FCD patterns after continuous irradiation under a UV lamp (365 nm) for 1 h; photograph of FCD powders under a 365 nm UV lamp excitation; photograph of the hydrolysis product of KH-792; fluorescence emission spectra of FCDs/SiO_2 nanocomposite powders with different concentrations of FCDs (λ_{ex} = 410 nm) (PDF)

DOI: 10.1021/acsomega.8b01919
ACS Omega 2018, 3, 13211−13218

AUTHOR INFORMATION

Corresponding Authors

*E-mail: wangdan@mail.buct.edu.cn. Phone: +86-10-64449453 (D.W.).

*E-mail: puyuan@mail.buct.edu.cn. Phone: +86-10-64421905 (Y.P.).

ORCID

Dan Wang: 0000-0002-3515-4590

Jie-Xin Wang: 0000-0003-0459-1621

Qiuqiang Zhan: 0000-0002-5886-3795

Notes

The authors declare no competing financial interest.

ACKNOWLEDGMENTS

We are grateful for the financial support from the National Key R & D Program of China (2016YFA0201701 and 2016YFA0201704), the National Natural Science Foundation of China (51641201, 61675071, 21808009), the Guangdong Provincial Science Fund for Distinguished Young Scholars (218B030306015) and the "111" project of China (B14004).

REFERENCES

(1) Yao, J.; Yang, M.; Duan, Y. Chemistry, Biology, and Medicine of Fluorescent Nanomaterials and Related Systems: New Insights into Biosensing, Bioimaging, Genomics, Diagnostics, and Therapy. *Chem. Rev.* **2014**, *114*, 6130−6178.

(2) Pu, Y.; Lin, L.; Wang, D.; Wang, J.-X.; Qian, J.; Chen, J.-F. Green Synthesis of Highly Dispersed Ytterbium and Thulium Co-doped Sodium Yttrium Fluoride Microphosphors for in Situ Light Upconversion from Near-infrared to Blue in Animals. *J. Colloid Interface Sci.* **2018**, *511*, 243−250.

(3) Wang, D.; Zhu, L.; Pu, Y.; Wang, J.-X.; Chen, J.-F.; Dai, L. Transferrin-coated Magnetic Upconversion Nanoparticles for Efficient Photodynamic Therapy with Near-infrared Irradiation and Luminescence Bioimaging. *Nanoscale* **2017**, *9*, 11214−11221.

(4) Leng, J.; Chen, J.; Wang, D.; Wang, J. X.; Pu, Y.; Chen, J.-F. Scalable Preparation of Gd_2O_3:Yb^{3+}/Er^{3+} Upconversion Nanophosphors in a High-Gravity Rotating Packed Bed Reactor for Transparent Upconversion Luminescent Films. *Ind. Eng. Chem. Res.* **2017**, *56*, 7977−7983.

(5) Li, D.; Wang, D.; Zhao, X.; Xi, W.; Zebibula, A.; Alifu, N.; Chen, J.-F.; Qian, J. Short-wave Infrared Emitted/Excited Fluorescence From Carbon Dots and Preliminary Applications in Bioimaging. *Mater. Chem. Front.* **2018**, *2*, 1343−1350.

(6) Wang, D.; Wang, Z. Y.; Zhan, Q. Q.; Pu, Y.; Wang, J. X.; Foster, N. R.; Dai, L. M. Facile and Scalable Preparation of Fluorescent Carbon Dots for Multifunctional Applications. *Engineering* **2017**, *3*, 402−408.

(7) Chen, J.-F. Green Chemical Engineering. *Engineering* **2017**, *3*, 283−284.

(8) Khan, S.; Verma, N. C.; Chethana; Nandi, C. K. Carbon Dots for Single-Molecule Imaging of the Nucleolus. *ACS Appl. Nano Mater.* **2018**, *1*, 483−487.

(9) Georgakilas, V.; Perman, J. A.; Tucek, J.; Zboril, R. Broad Family of Carbon Nanoallotropes: Classification, Chemistry, and Applications of Fullerenes, Carbon Dots, Nanotubes, Graphene, Nanodiamonds, and Combined Superstructures. *Chem. Rev.* **2015**, *115*, 4744−4822.

(10) Lim, S. Y.; Shen, W.; Gao, Z. Carbon Quantum Dots and Their Applications. *Chem. Soc. Rev.* **2015**, *44*, 362−381.

(11) Dang, H.; Huang, L.-K.; Zhang, Y.; Wang, C.-F.; Chen, S. Large-Scale Ultrasonic Fabrication of White Fluorescent Carbon Dots. *Ind. Eng. Chem. Res.* **2016**, *55*, 5335−5341.

(12) Wang, D.; Chen, J.-F.; Dai, L. Recent Advances in Graphene Quantum Dots for Fluorescence Bioimaging from Cells through Tissues to Animals. *Part. Syst. Char.* **2015**, *32*, 515−523.

(13) Fernando, K. A. S.; Sahu, S.; Liu, Y.; Lewis, W. K.; Guliants, E. A.; Jafariyan, A.; Wang, P.; Bunker, C. E.; Sun, Y.-P. Carbon Quantum Dots and Applications in Photocatalytic Energy Conversion. *ACS Appl. Mater. Interfaces* **2015**, *7*, 8363−8376.

(14) LeCroy, G. E.; Sonkar, S. K.; Yang, F.; Veca, L. M.; Wang, P.; Tackett, K. N.; Yu, J.-J.; Vasile, E.; Qian, H.; Liu, Y.; Luo, P.; Sun, Y.-P. Toward Structurally Defined Carbon Dots as Ultracompact Fluorescent Probes. *ACS Nano* **2014**, *8*, 4522−4529.

(15) Jiang, K.; Wang, Y.; Gao, X.; Cai, C.; Lin, H. Facile, Quick, and Gram-Scale Synthesis of Ultralong-Lifetime Room-Temperature-Phosphorescent Carbon Dots by Microwave Irradiation. *Angew. Chem., Int. Ed.* **2018**, *57*, 6216−6220.

(16) Bacon, M.; Bradley, S. J.; Nann, T. Graphene Quantum Dots. *Part. Part. Syst. Char.* **2014**, *31*, 415−428.

(17) Pal, T.; Mohiyuddin, S.; Packirisamy, G. Facile and Green Synthesis of Multicolor Fluorescence Carbon Dots from Curcumin: In Vitro and in Vivo Bioimaging and Other Applications. *ACS Omega* **2018**, *3*, 831−843.

(18) Zheng, Y.; Xie, G.; Zhang, Xu.; Chen, Z.; Cai, Y.; Yu, W.; Liu, H.; Shan, J.; Li, R.; Liu, Y.; Lei, B. Bioimaging Application and Growth-Promoting Behavior of Carbon Dots from Pollen on Hydroponically Cultivated Rome Lettuce. *ACS Omega* **2017**, *2*, 3958−3965.

(19) Atchudan, R.; Edison, T. N. J. I.; Sethuraman, M. G.; Lee, Y. R. Efficient Synthesis of Highly Fluorescent Nitrogen-Doped Carbon Dots for Cell Imaging Using Unripe Fruit Extract of Prunus Mume. *Appl. Surf. Sci.* **2016**, *384*, 432−441.

(20) So, R. C.; Sanggo, J. E.; Jin, L.; Diaz, J. M. A.; Guerrero, R. A.; He, J. Gram-Scale Synthesis and Kinetic Study of Bright Carbon Dots from Citric Acid and Citrus japonica via a Microwave-Assisted Method. *ACS Omega* **2017**, *2*, 5196−5208.

(21) Khare, P.; Bhati, A.; Anand, S. R.; Gunture; Sonkar, S. K. Brightly Fluorescent Zinc-Doped Red-Emitting Carbon Dots for the Sunlight-Induced Photoreduction of Cr(VI) to Cr(III). *ACS Omega* **2018**, *3*, 5187−5194.

(22) Claeys, W. L.; Cardoen, S.; Daube, G.; De Block, J.; Dewettinck, K.; Dierick, K.; De Zutter, L.; Huyghebaert, A.; Imberechts, H.; Thiange, P.; Vandenplas, Y.; Herman, L. Raw or Heated Cow Milk Consumption: Review of Risks and Benefits. *Food Control* **2013**, *31*, 251−262.

(23) Wang, L.; Zhou, H. S. Green Synthesis of Luminescent Nitrogen-Doped Carbon Dots from Milk and Its Imaging Application. *Anal. Chem.* **2014**, *86*, 8902−8905.

(24) Wang, D.; Wang, X.; Guo, Y.; Liu, W.; Qin, W. Luminescent Properties of Milk Carbon Dots and Their Sulphur and Nitrogen Doped Analogues. *RSC Adv.* **2014**, *4*, 51658−51665.

(25) Wang, D.; Zhu, L.; Mccleese, C.; Burda, C.; Chen, J.-F.; Dai, L. Fluorescent Carbon Dots from Milk by Microwave Cooking. *RSC Adv.* **2016**, *6*, 41516−41521.

(26) Pham-Truong, T.-N.; Petenzi, T.; Ranjan, C.; Randriamahazaka, H.; Ghilane, J. Microwave Assisted Synthesis of Carbon Dots in Ionic Liquid as Metal Free Catalyst for Highly Selective Production of Hydrogen Peroxide. *Carbon* **2018**, *130*, 544−552.

(27) Liu, J.; Chen, P.; Yao, W. J.; Wang, J.; Wang, L.; Deng, L.; He, J.; Zhang, G.; Lei, J. Subcritical Water Extraction of Betulinic Acid from Birch Bark. *Ind. Crop. Prod.* **2015**, *74*, 557−565.

(28) Toor, S. S.; Rosendahl, L.; Rudolf, A. Hydrothermal Liquefaction of Biomass: A Review of Subcritical Water Technologies. *Energy* **2011**, *36*, 2328−2342.

(29) Islam, M. N.; Taki, G.; Rana, M.; Park, J.-H. Yield of Phenolic Monomers from Lignin Hydrothermolysis in Subcritical Water System. *Ind. Eng. Chem. Res.* **2018**, *57*, 4779−4784.

(30) Pirmoradi, M.; Kastner, J. R. Synthesis of Methacrylic Acid by Catalytic Decarboxylation and Dehydration of Carboxylic Acids Using a Solid Base and Subcritical Water. *ACS Sustainable Chem. Eng.* **2017**, *5*, 1517−1527.

(31) Rynne, N. M.; Beresford, T. P.; Kelly, A. L.; Guinee, T. P. Effect of Milk Pasteurization Temperature and in Situ Whey Protein

DOI: 10.1021/acsomega.8b01919
ACS Omega 2018, 3, 13211−13218

Denaturation on the Composition, Texture and Heat-induced Functionality of Half-fat Cheddar Cheese. *Int. Dairy J.* **2004**, *14*, 989−1001.
(32) Shelver, W. L.; Lupton, S. J.; Shappell, N. W.; Smith, D. J.; Hakk, H. Distribution of Chemical Residues among Fat, Skim, Curd, Whey, and Protein Fractions in Fortified, Pasteurized Milk. *ACS Omega* **2018**, *3*, 8697−8708.
(33) O'Brien, J.; Morrissey, P. A.; Ames, J. M. Nutritional and toxicological aspects of the Maillard browning reaction in foods. *Crit. Rev. Food Sci. Nutr.* **1989**, *28*, 211−248.
(34) Wang, N.; Wang, Y.; Guo, T.; Yang, T.; Chen, M.; Wang, J. Green Preparation of Carbon Dots with Papaya as Carbon Source for Effective Fluorescent Sensing of Iron (III) and Escherichia coli. *Biosens. Bioelectron.* **2016**, *85*, 68−75.
(35) Ding, H.; Yu, S.-B.; Wei, J.-S.; Xiong, H.-M. Full-Color Light-Emitting Carbon Dots with a Surface-State-Controlled Luminescence Mechanism. *ACS Nano* **2016**, *10*, 484−491.
(36) Yang, X.; Zhuo, Y.; Zhu, S.; Luo, Y.; Feng, Y.; Dou, Y. Novel and Green Synthesis of High-fluorescent Carbon Dots Originated from Honey for Sensing and Imaging. *Biosens. Bioelectron.* **2014**, *60*, 292−298.
(37) Chen, Y.; Yang, Q.; Xu, P.; Sun, L.; Sun, D.; Zhuo, K. One-Step Synthesis of Acidophilic Highly-Photoluminescent Carbon Dots Modified by Ionic Liquid from Polyethylene Glycol. *ACS Omega* **2017**, *2*, 5251−5259.
(38) Zhou, J.; Sheng, Z.; Han, H.; Zou, M.; Li, C. Facile synthesis of fluorescent carbon dots using watermelon peel as a carbon source. *Mater. Lett.* **2012**, *66*, 222−224.
(39) Liu, S.; Tian, J.; Lei, W.; Zhang, Y.; Qin, X.; Luo, Y. Hydrothermal treatment of grass: a low-cost, green route to nitrogen-doped, carbon-rich, photoluminescent polymer nanodots as an effective fluorescent sensing platform for label-free detection of cu(ii) ions. *Adv. Mater.* **2012**, *24*, 2037−2041.
(40) Mehta, V. N.; Jha, S.; Basu, H.; Singhal, R. K.; Kailasa, S. K. One-step hydrothermal approach to fabricate carbon dots from apple juice for imaging of mycobacterium and fungal cells. *Sens. Actuators, B* **2015**, *213*, 434−443.
(41) Kasibabu, B. S. B.; D'Souza, S. L.; Jha, S.; Singhal, R. K.; Basu, H.; Kailasa, S. K. One-step synthesis of fluorescent carbon dots for imaging bacterial and fungal cells. *Anal. Methods* **2015**, *7*, 2373−2378.
(42) Huang, H.; Li, C.; Zhu, S.; Wang, H.; Chen, C.; Wang, Z.; Bai, T.; Shi, Z.; Feng, S. Histidine-derived Nontoxic Nitrogen-doped Carbon Dots for Sensing and Bioimaging Applications. *Langmuir* **2014**, *30*, 13542.
(43) Li, S.; Chen, D.; Zheng, F.; Zhou, H.; Jiang, S.; Wu, Y. Water-Soluble and Lowly Toxic Sulphur Quantum Dots. *Adv. Funct. Mater.* **2014**, *24*, 7133−7138.
(44) Wang, J.; Zhang, F.; Wang, Y.; Yang, Y.; Liu, X. Efficient Resistance Against Solid-state Quenching of Carbon Dots towards white Light Emitting Diodes by Physical Embedding into Silica. *Carbon* **2018**, *126*, 426−436.
(45) Pu, Y.; Wen, X.; Li, Y.; Wang, D.; Foster, N. R.; Chen, J.-F. Ultrafine Clarithromycin Nanoparticles Via Anti-solvent Precipitation in Subcritical Water: Effect of Operating Parameters. *Powder Technol.* **2017**, *305*, 125−131.

DOI: 10.1021/acsomega.8b01919
ACS Omega 2018, 3, 13211−13218